



Combustion characteristics of stoichiometric Al-CuO nanocomposite thermites prepared by different methods

I. Monk, M. Schoenitz, R.J. Jacob, E.L. Dreizin & M.R. Zachariah

To cite this article: I. Monk, M. Schoenitz, R.J. Jacob, E.L. Dreizin & M.R. Zachariah (2016): Combustion characteristics of stoichiometric Al-CuO nanocomposite thermites prepared by different methods, Combustion Science and Technology, DOI: [10.1080/00102202.2016.1225731](https://doi.org/10.1080/00102202.2016.1225731)

To link to this article: <http://dx.doi.org/10.1080/00102202.2016.1225731>



Accepted author version posted online: 22 Aug 2016.
Published online: 22 Aug 2016.



Submit your article to this journal [↗](#)



View related articles [↗](#)



View Crossmark data [↗](#)

Combustion characteristics of stoichiometric Al-CuO nanocomposite thermites prepared by different methods

Monk, I.¹, Schoenitz, M.¹, Jacob, R.J.², Dreizin, E.L.¹, Zachariah, M.R.²

¹New Jersey Institute of Technology, Newark, NJ 07102

²University of Maryland, College Park, MD 20742

Corresponding author: E.L. Dreizin, dreizin@njit.edu, 973-596-5751

Abstract

Three nanocomposite materials with the same nominal stoichiometric thermite composition of 2Al-3CuO were prepared by three different methods: ultrasonic mixing of constituent nanopowders (USM), electro spraying (ES) and arrested reactive milling (ARM). Prepared powders were placed in a 6.7-mm diameter, 0.5-mm deep cavity in a brass substrate and ignited by electro-static discharge. The experiments were performed in air, argon, and helium. The mass of powder removed from the sample holder after ignition was measured in each test. Using a multi-anode photomultiplier tube coupled with a spectrometer, time-resolved light emission traces produced by the ignited samples were recorded in the range of wavelengths of 373-641 nm. Time-resolved temperatures were then determined by fitting the recorded spectra assuming Planck's black body emission. Temporal pressure generated by ignition events in the enclosed chamber showed that the powder's combustion properties were tied to both their preparation technique as well as the environment they were ignited in. We found that agglomeration of nanoparticles hindered combustion of USM powders; while it was not observed for the ES powders. In oxygen-free gas environments, lower temperatures and pressures were observed for USM and ES powders prepared using starting nano-particles. For the ES powders, the effect of gas environment was less significant, which was interpreted considering that ES materials

included gasifying nitrocellulose binder, enhancing heat and mass transfer between individual Al and CuO particles. Higher pressures and temperatures were observed in inert environments for the ARM-prepared powder.

Keywords: ultrasonic mixing, electrospray, arrested reactive milling, electro-static discharge, ignition, agglomeration.

Introduction

Nanocomposite thermites have attracted attention recently due to a range of potential applications, especially those in pyrotechnics (Spitzer et al. 2010, Comet, Pichot, et al. 2010, Comet, Siegert, et al. 2010, Dreizin 2009, Reese, Wright, and Son 2013). Their fast energy release combined with high energy densities make nano-thermites more attractive than conventional thermites made of micron-scale powder particles (Pantoya and Granier 2005, Kim and Zachariah 2004, Yetter, Risha, and Son 2009). The increased reactivity of nanocomposite thermite is due to a highly developed interface between metal fuel, typically aluminum, and an oxidizer comprising a metal oxide, most commonly, CuO, Fe₂O₃, MoO₃, Bi₂O₃, etc.

Several methods have been recently developed to prepare nanocomposite thermites, with each method imparting specific structural characteristics to the generated nanocomposite. The most common technique employs physically mixing nanopowders of individual components (Sun, Pantoya, and Simon 2006, Sanders et al. 2007). The powder is suspended in a liquid, commonly hexane, and is mixed using ultrasonic agitation, following which the liquid is evaporated. The produced materials, often referred to as metastable intermolecular composites or MIC's, are explored as potential reactive or energetic materials. Due to the inherent agglomeration of the as produced nanopowders, MIC samples can exhibit poor mixing at the nanoscale if such

agglomerates are not broken up during the ultra-sonication. Moreover, during the evaporation of the solvent fuel and oxidizer nanopowders may re-agglomerate preferentially, leading to a poorly mixed composite. A modified method for enhancing the nanoscale mixing of nanopowders involves the addition of an organic binder to the ultrasonicated mixture of nanopowders. The generated suspension is dispersed into an aerosol using an electrospray (Wang et al. 2014, Li et al. 2015) which generates uniformly sized ($<10\ \mu\text{m}$) droplets of the suspension. When the solvent dries from the electrosprayed droplets, it leaves behind a composite particle, held together by the binder. The resulting composite particles are micron-sized ($\sim 1\ \mu\text{m}$) albeit mixed at the nanoscale and offer processing advantages compared to nanopowders. Upon ignition, the binder is gasified at a temperature below the ignition temperature of the nano-thermite, causing particle-particle separation, which is thought to diminish sintering and rapid loss of reactive surface area (Jacob, Wei, and Zachariah 2015). Yet another method for the preparation of well mixed nanocomposite material is Arrested Reactive Milling or ARM (Dreizin and Schoenitz 2009), which uses high energy ball milling of starting micron-sized components, to prepare fully dense composite powders. Sizes of produced composite powder particles vary in the range of $1 - 100\ \mu\text{m}$ with each particle containing starting materials mixed on the nanoscale.

This work is aimed to characterize the similarities and differences between combustion behaviors of reactive materials comprising a nanocomposite thermite: stoichiometric Al-CuO (2:3 per mole basis), prepared in three distinct ways. The methods of preparation include traditional ultrasonic mixing (USM) of nano-powders (Son et al. 2007, Dutro et al. 2009, Reese, Wright, and Son 2013, Bockmon et al. 2005), electrospraying (ES) (Wang et al. 2014, Wang et al. 2015, Young, Wang, and Zachariah 2015, Jacob, Wei, and Zachariah 2015), and ARM (Schoenitz, Ward, and Dreizin 2005, Dreizin and Schoenitz 2009, Dreizin and Schoenitz 2014). The results are

expected to emphasize the effect of the material structure and morphology on its ignition and combustion. Such material comparisons are needed to guide further developments in the reactive material preparation technologies as well as to enable fine-tuning of specific characteristics of different materials.

Materials

The ES and USM composites were created using 50-nm copper oxide from Sigma-Aldrich and 50-nm aluminum from Argonide Corporation (70% active). The USM materials were prepared through the ultrasonication of copper oxide in ethanol for 1 hr. before aluminum was added; whereby an additional 1 hr. of ultrasonication was performed to ensure good physical mixing of particles. The material was sieved to break up large agglomerates. For the ES composites, the precursor mixing procedure was similar. Collodion solution of 4-8wt.% nitro cellulose in ethanol/diethyl ether (Sigma-Aldrich) was diluted with a diethyl ether (99.8%)/ethanol (99.8%) mixture (1:3 volume ratio) to which stoichiometric mixture of aluminum and copper oxide was added, limiting the nitrocellulose content to 5 wt. % of the total solids loading. The mixture was sonicated for an hour followed by 24 hours of magnetic stirring. The precursor solution was subsequently loaded into a syringe pump and electro sprayed onto an aluminum foil. The foil was placed at a suitable distance away from the needle such that the field necessary for the electro spray was maintained as well as sufficient transit time was available for the solvent in the droplet to evaporate. The sprayed composite powder was subsequently harvested off the foil for further experiments. A more detailed explanation of the process can be found in Ref. (Wang et al. 2014).

The ARM materials were prepared as described elsewhere (Schoenitz, Ward, and Dreizin 2005). The starting materials were -325 mesh (less than 44 μm), 99.5% pure aluminum by Atlantic

Equipment Engineers and 25 μm , 99+% pure copper (II) oxide by Sigma Aldrich. A Retsch PM400 planetary mill was used with custom-made thick-walled hardened steel vials. The Al and CuO were milled using 9.525 mm (3/8") diameter hardened steel balls with the ball to powder mass ratio of 3:1. Hexane was used as a process control agent (24 mL per vial). The material was milled for approximately 60 min and stored under hexane. The powder used in the experiments was stored for up to 2 years. Its reaction was preliminarily examined using differential scanning calorimetry (DSC) in argon, which showed no detectable effect of aging on the observed thermite reactions.

Figure 1 shows scanning electron microscope (SEM) images of all three types of thermite powders. The images were taken using backscattered electrons which offered brightness contrast based on the molecular weight of the involved phases. The brightness difference between Al and CuO is detectable, with CuO particles generally appearing slightly brighter than Al owing to the larger atomic mass of copper. Mixing between Al and CuO appears to be somewhat more homogeneous for ES and USM materials compared to the ARM-prepared composite. Individual inclusions of CuO in the ARM material are slightly coarser than particles of CuO in both ES and USM composites. USM composite appears to be most porous, although substantial porosity is also observed in the ES particles. Conversely, most of the ARM particles are fully dense.

Combustion experiments

All powders were ignited using an experimental setup based on a 931 model Firing Test System by Electro-Tech Systems, Inc. The experiment was discussed in detail earlier (Williams, Patel, and Dreizin 2014, Williams, Beloni, and Dreizin 2012, Monk et al. 2015) and only a brief summary is given here.

The powders were loaded to completely fill a 0.5-mm deep, 6.7-mm diameter cylindrical void in a brass sample holder. Excess powder was removed using a razor blade to ensure a flat top surface. The mass of the loaded powder depended on porosity of the sample. The mass loads of the ES, USM, and ARM composites varied in the ranges of 3.87 – 4.53, 6.11 - 7.21, and 16.4 – 19.4 mg, respectively. The powder-filled sample holder was placed 1 mm away from the pin-electrode. Experiments were performed inside a sealed chamber ($6.24 \times 10^{-4} \text{ m}^3$) filled with air, argon, or helium up to 101.325 kPa. For experiments in argon and helium, the chamber was evacuated to 67.7 kPa and then filled with the corresponding gas. This process was repeated three times to minimize the oxygen concentration down to 1.55 mol/m^3 or to a total of $8.85 \times 10^{-4} \text{ mol}$ of oxygen in the chamber. In most experiments, the electro-static discharge (ESD) was produced by discharge of a 2000-pF capacitor, preliminarily charged to a voltage of 10 kV. To ignite the ES powder in helium, it was necessary to increase the voltage to 20 kV and use a 10000-pF capacitor (all ES He runs will be noted by an asterisk* throughout the paper). The capacitor discharge was triggered electronically. Three runs were performed for each environment and powder for a total of nine runs per powder.

Aluminum foil preliminarily cleaned with acetone was mounted onto SEM stubs using double-sided carbon tape to collect combustion products. The foil was placed 18-22 mm from the powder-loaded sample holder. All parts of the ESD apparatus were cleaned with acetone prior to each test to avoid cross contamination between products of different materials. Samples were weighed before and after ignition using an Acculab ALC-80.4 balance, in order to determine the amount of powder removed from the sample holder and thus participated in each combustion event.

Emission signals produced by ignited materials were collected using a 32-channel spectrometer based on a Hamamatsu H7260 series linear array multi-anode photo-multiplier tube (PMT). The wavelengths for the 32 channels were in the range of 373.4 - 641.0 nm. The time resolution of the individual emission traces recorded for each wavelength was 5 μ s, which was determined by the National Instruments PCI-6133 DAQ-boards used for data acquisition. National Instrument's Labview 8.5 software was used to collect the data; the results were processed using a customized code in MATLAB. The data processing included calculation of the temperature based on the recorded spectrally resolved emission traces using Planck's formula. The spectrometer output was calibrated using a tungsten filament lamp and a NIST traceable StellarNet EPP-2000 spectrometer. Additional details are available elsewhere (Monk, Schoenitz, and Dreizin 2016). Pressure measurements were made using a PCB Piezotronics Model 106B51 Pressure Transducer installed in the ESD chamber and connected to a PCB Model 482A21 signal conditioner and to a LeCroy WaveSurfer 64Xs Series oscilloscope.

Results

Material ejected from the sample holder

Fractions of the powder mass ejected from the sample holder for different materials are shown in Table 1. It is observed that most of the loaded powder was ejected and thus expected to burn in all experiments. However, it is unclear whether the reaction was complete for all materials. The effect of gas environment on the fraction of the powder ejected from the sample holder is relatively minor. Note that the absolute masses of the powders ejected for each material are affected by the density of the sample. The densities are also shown in Table 1; the ARM-prepared powder has the highest density, followed by the USM, and then by ES materials.

Emission Data

An example of the light emission traces collected using the 32-channel spectrometer is shown in Fig. 2. The emission pulses produced by the spark itself were no longer than 5 – 6 μs , i.e., they were much shorter than the traces shown. Emission intensity peaks between 500 and 600 nm. It is also apparent that the emission at longer wavelengths becomes stronger for longer times, indicating a decreasing temperature. For clarity, comparisons between different types of thermite powders are illustrated in Fig. 3 using one selected emission trace corresponding to 567.7 nm. This wavelength was chosen due to its similarity to the filtered emission traces recorded in previous experiments (Monk, Schoenitz, and Dreizin 2016, Monk et al. 2015). It is also not expected to interfere significantly with molecular emission bands of AlO (Goroshin et al. 2007). Typical traces of all three composite powders (ES, USM, and ARM) ignited in various environments (air, argon, and helium) are shown in Fig. 3. Signal amplitudes differ, with the signal produced in air being the strongest for all powders. Comparison of pulse amplitudes for different materials may be misleading because of systematic difference in the total amount of burning material caused by the difference in densities among different types of powders filling the sample holder. As shown in Table 1, the density was highest for the ARM-prepared powder. Respectively, more material was loaded and ignited in each test, causing stronger overall emission intensity.

The signals peak at the shortest times for the USM powder; the peak position is most delayed for the ES material (except for ignition in He, when a higher ESD energy was used). It appears that the preparation method has a stronger effect on the temporal position of the peak intensity than the gas environment.

Collected 567.5-nm emission traces were processed to establish their main temporal characteristics. The parameters of interest include peak onset (determined by the first peak of the

signal's time derivative), peak position (determined at 100% of the peak height or t_{100}), peak width (determined as the time while the signal exceeds 50% of its peak value or period between times $t_{.50}$ and $t_{+.50}$), and burn time (determined when the signal decreases to 10% of its peak value, t_{10}). The processing results are shown in Fig. 4. Note the logarithmic time scale when comparing times. The peak onset times as well as $t_{.50}$ and t_{100} are the longest for the ES and the shortest for the USM powders, except for the ES powder in helium, when a higher ESD energy (20 kV, 10000 pF) was used. In that latter case, all three initial characteristic times occur much earlier, although the overall duration of the emission pulse is nearly the same for all materials. The pulses observed in helium are shorter than in air or argon for all materials. For ES and USM powders, the emission traces ended at approximately the same time in both air and argon. For ARM-prepared powder, the trace in argon was longer. For all materials, the pulse width is greater in air than in inert gas environments. In air, the pulse width is greater and peak position is further delayed for the ES material. The narrowest pulse and shortest peak position delay (t_{100}) is observed for the USM powders for all environments.

Temperature and Pressure Data

Emissivity was assumed independent of the wavelength to obtain black body emission temperatures using all 32 recorded filtered emission traces. A wavelength-dependent emissivity, e.g., following a $\epsilon \sim \lambda^{-2.94}$ trend (Dreizin, Allen, and Glumac 2014) was considered; however, the goodness of fit for the respective Planck's curves was substantially reduced; thus the gray body assumption was maintained. Figure 5 shows a typical 32-channel trace for ARM powder in air overlaid with the respective temperature. The error bars for temperature indicate 95% confidence intervals. The temperature peaks when the emission intensity is increasing, at around 400 μ s. The peak temperature is about 2830 K, close to the adiabatic temperature of 2810 K predicted for the

stoichiometric Al-CuO reaction by the CEA equilibrium code (McBride and Gordon 1996). The temperature is reduced to about 2500 K by 1 ms, when most emission traces are close to their maximum values. The presently measured temperatures are slightly higher than 2250 – 2400 K, the range of temperatures measured for the USM-prepared Al-CuO nanothermites burning in an unconfined pile or in an open tube (Weismiller, Lee, and Yetter 2011). Furthermore, the present temperatures exceed ca. 2300 K obtained for individual ARM-prepared $2\text{Al}-3\text{CuO}$ particles (Dreizin et al. 2011). Qualitatively, the temperature traces appeared to be similar to one another for all materials. Therefore, no additional temperature traces are shown.

For comparisons between materials, the single temperature value taken at the peak position (t_{100}) of the emission trace filtered at 567.7 nm was considered for all samples. Temperatures for different powders ignited in different gas environments are shown in Fig. 6. For ARM materials, temperatures in air are somewhat lower than those reported for argon and helium. Conversely, for USM and ES powders, the temperatures measured in air are higher than those observed in inert gas environments. The effect of environment on temperature is weaker for ES than for USM powder.

Pressures recorded for different powders ignited in air are shown in Fig. 7 along with filtered 567.7-nm emission traces. The pressures are normalized per unit mass of the powder ejected from the sample holder, and thus expected to participate in the reaction. Therefore, normalized pressures shown can be directly compared for different types of powders. The pressure signals are expected to be delayed from the emission by the time the sound wave needs to travel from the ignited powder to the pressure transducer. This time can be estimated as approximately 0.6 ms, assuming the speed of sound in the chamber to be 340 m/s and the distance to the pressure transducer to be close to the chamber characteristic dimension, e.g., 20 cm. Indeed, the pressure

trace begins after a 0.6-0.7 ms delay. However, the pressure peak is observed some 10 ms following the peak of the emission signal, indicating a truly delayed signal. This delay suggests that the exothermic reaction continues for the entire duration of the observed emission signal, even during its decay, causing further heating of the gas inside the chamber. This heating of the gas in an enclosed chamber combined with the release of gas-phase combustion products creates the respective pressure rise. Oscillatory patterns observed in the pressure traces occur with an approximately 0.5-ms period, and thus are likely to represent reflections of the sound wave within the chamber. The oscillations are stronger for signals with higher overall pressures. The temporal characteristics of pressure traces are summarized in Fig. 8, similar to the analogous plot for the emission traces in Fig. 4. The onset of the pressure pulse occurs sooner for USM materials, except for the case of ES powder ignited in He, when a higher voltage was used. Aside from the case of ES powder ignited in He, the onset of the pressure pulse occurs sooner in air than in inert gases. The pressure peak positions (t_{100}) follow the same trend for all materials: pressures first peak in He, then in air, and finally in Ar. For the ES powder, despite a delayed pressure peak position observed in Ar, the overall pressure signal in Ar is shorter than in other gases. Conversely, for ARM powder the duration of pressure peak in Ar is much longer than in air and He. For USM powder, the pressure peaks have approximately the same duration in Ar and air; the peak in He is much shorter.

Pressure peak values normalized per unit mass of the ignited material are compared for different powders in Fig. 9. The effect of gas environment is different for different powders. For USM powders, the highest pressure is observed in air. Ignition becomes difficult for this sample in Ar; very low pressures were observed in some tests, causing a very large error bar. Conversely, in He, USM powder ignited readily and generated pressure that was nearly as high as in air. For the

ARM powder, the pressure in air is lower than in both Ar and He. In both inert gases, the pressures for ARM powder are close to each other. This trend correlates well with that observed for the temperatures for this powder in Fig. 6, which are also higher in inert gases. The ES powders generated the highest mass normalized pressures in both air and Ar; however, they did not ignite in He when the same ESD energy was used. When an increased ESD voltage was applied, ignition occurred and the normalized pressure was substantially higher than for other materials.

Combustion product morphology

Particles ignited in air were collected and examined under SEM. Characteristic images for ES-prepared, USM, and ARM particles are shown in Fig. 10. In addition to relatively coarse particles as shown in Fig. 10, much finer spheres, representing typical smoke particles, were observed for all materials; few such particles can be seen in Fig. 10A.

In Fig. 10, a particle most representative of the combustion products was selected among many acquired SEM images for each material. For all combustion product particles, phases containing primarily Al_2O_3 (darker gray in SEM images) and Cu (bright) can be readily distinguished. In many cases, Cu-rich phase forms a characteristic “cap”, somewhat similar to an oxide cap observed on quenched aluminum particles (Dreizin 1996, Jacob et al. 2015). Prevalent particle sizes are different for products of different materials. The finest particles were observed for the ES powders; the particle size varied in the range of 1 – 2 μm consistently with earlier observations (Wang et al. 2014). For both ARM and USM powders, particles were mostly coarser, with a characteristic dimension in the order of 10 μm . It appears that the morphology of the original composite material is completely lost for both ARM and ES powders. The particle shapes, scale of mixing among products, and surface morphology are likely representative of

cooling fairly well homogenized mixed molten products. However, in Fig. 10B, an agglomerate of original aluminum nano-particles can be distinguished for the USM powder. The agglomerated particles appear to be “bonded” together with a brighter, Cu-rich melt, apparently percolating through the pores in the initially agglomerated particles.

Discussion

It is of interest to consider similarities and differences in the ignition and combustion behaviors among 2Al—3CuO powders prepared by different methods and ignited by ESD. Further, the present results can be compared to earlier measurements, employing the same technique for igniting nanothermite powders (Monk, Schoenitz, and Dreizin 2016) as well as to reports describing combustion of Al-CuO nanocomposite ignited in different experimental configurations (Weismiller, Lee, and Yetter 2011, Dreizin et al. 2011). To set the framework for the discussion, consider the following events induced by the ESD discharge striking a powder sample. First, the spark produces a shockwave and heated plasma that aerosolizes some of the powder. The size of the aerosol cloud is between 2 and 3 cm, depending on the ESD energy and the density of the powder. Most of the lifted powder is cold, although a fraction of particles that was hit by the spark directly is heated and ignited nearly instantaneously. These directly heated particles begin reacting within single microseconds following the spark discharge. These times are typically shorter than necessary for the temperature to equilibrate across particles or agglomerates with dimensions of tens of μm . Thus, the nano-structure of such particles or agglomerates is preserved during their ignition. The heat from the ignited and burning particles ignites the rest of the aerosol, which occurs with a delay caused by the time necessary for the heat to propagate through the powder cloud. This delay is typically of the order of tens of ms; thus aluminum in the composite material melts causing sintering for USM powder or loss of

nano-structure for the ARM-prepared material. Therefore, once ignited, many such particles will have lost their nanostructure. Presence of nitrocellulose in the ES powder may prevent or delay the particle sintering. The ignited powder cloud generates additional convective flow, which lifts more powder. The newly lifted powder ignites once it is being mixed with the burning powder. Once again, the ignition delays are long enough for the nanostructure to be lost upon ignition. Temporal characteristics of the optical emission traces summarized in Fig. 4 for different materials can be correlated with events occurring in respective combustion experiments. The initial ignition delay, reflecting ignition of particles heated directly by ESD is best represented by the initial emission onset time, shown for all materials in Fig. 4. Aside from the experiment with ES powder in He, when a higher ESD power was used, the delays are longer for ES powder, indicating most likely a slower initial low-temperature solid-solid reaction between Al and CuO, which may be separated in this material by binder. Heating of the ES powder by the spark current could also have been less effective because of its greater electrical resistance. When the ESD energy is increased, for the ES powder ignited in He, the emission onset time is markedly reduced, suggesting that the particles were preheated to a much higher temperature during the ESD pulse.

When multiple aerosolized particles are ignited, combustion products may remain incandescent for an extended period of time, because they form a relatively large cloud. Thus, the total emission time is representative of the time scale describing heat and mass transfer from the burning powder cloud.

The peak of the optical emission signal may represent both growth of the cloud size and/or density and increased rate of reaction for the burning particles. Setting aside the case of ES powder in He, when a greater ESD energy was used, the peaks of emission occur at the shortest

times for USM powders and at longest times for the ES powder, with the ARM powder being in the middle for all environments, mirroring the trend observed for the emission onset. Because the mass of ARM powder loaded in the sample holder was the greatest, it formed the densest clouds. This is consistent with the strongest emission signal observed for this powder (see Fig. 3). Therefore, the densest cloud produced by the ARM powder generated its strongest emission signal earlier than that generated by the lowest density cloud produced by ES powder. This observation can be interpreted assuming that the cloud combustion rate is affected by the ignition rates of individual particles, which are lower for the ES powder, as mentioned above. For USM powder, the reaction slows down early, most likely because it is incomplete and because agglomerated particles, such as shown in Fig. 10b, extinguish.

The end of incandescence is expected to indicate the cooling of the cloud and end of the reaction; however, interpreting this incandescence is difficult because it is also affected by both size and brightness of the cloud. Conversely, the measured pressure traces represent fairly accurately the heat released in the reaction; the effect of gas products is expected to be comparatively weak for the present thermite combustion experiments. The presence of nitrocellulose in the ES material is also not expected to affect pressure significantly. Based on the mass of powder and nitrocellulose percentage added (5 %), only about 0.2 mg of nitrocellulose was included in an individual ES powder load. It roughly translates into $5 \cdot 10 \cdot 10^{-5}$ moles of gas if fully gasified. The chamber contained close to $2.5 \cdot 10^{-2}$ moles of air, and thus an additional pressure caused by gasification of nitrocellulose would only change the total pressure by about 0.02-0.04%. The primary cause for pressure increase is the heat release; thus, the peak of the recorded pressure signal represents the end of the exothermic reaction rather accurately. Indeed, the peak pressure roughly coincides with the end of the optical emission trace for all powders (Fig. 7).

It is interesting that the peak pressures occur at approximately the same times for all powders ignited in He. The trend in Fig. 8, showing the peak position as a function of the gas environment is also the same for all powders. The times are shortest in He (~ 2 ms) and longest in Ar (7 – 15 ms). It may suggest that the duration of a combustion event is correlated with the time of heat and mass transfer over the volume occupied by the ejected powder cloud, which is roughly the same for all powders. The durations of the combustion events for all samples are similar to those measured for individual ARM-prepared Al-CuO particles in Ref. (Dreizin et al. 2011). This observation suggests that for ARM-prepared powders, the burn times of individual particles may be close to the characteristic transport time in the cloud of the ESD-ejected powder. However, the present burn times are much longer than reported for ES and USM materials, ignited in a miniature combustion cell (Wang et al. 2014).

The effect of environment on the maximum pressure (Fig. 9) and temperature (Fig. 6) is qualitatively different for ARM powder compared to both ES and USM materials. For both ES and USM powders, both pressure and temperature are higher in air than in either argon or helium. This suggests a significant role of ambient oxygen reacting with aluminum. Conversely, for ARM powder the pressure and temperature are lower in air as compared to both inert gases. Because of the structure of the ARM-produced particles, their reaction with ambient oxygen is expected to be insignificant. The reduction in the pressure and temperature in air may be associated for the ARM material with re-oxidation of partially reduced CuO (e.g., forming Cu₂O) and possible formation of ternary oxide phases separating Al from CuO, such as Al₂CuO₄, which may slow down further thermite reaction. The temperatures inferred from the emission traces for all materials are close to those reported earlier for similar nanothermites (Weismiller, Lee, and Yetter 2011, Dreizin et al. 2011) ignited in different experimental configurations. The difference

in the temperatures observed for different powders in various environments may be caused by both pressure wave affecting ejection of unignited powder, the rate of heat loss from the burning particle cloud to the rest of the chamber, and also by the mass of the burning material. A difference in the initial density of differently prepared powder samples may affect their ejection, and thus affect the measured temperature. The low density of ES powder may therefore explain the slightly lower temperatures observed for this material in Ar and He, when much smaller amounts of this powder are being ejected and thus produce clouds, which cool faster despite the relatively low thermal diffusivity of Ar.

Differences in the observed combustion behavior can be correlated with morphologies of the combustion products collected for different powders. Dimensions of agglomerates observed in the as prepared USM powder (Fig. 1B) are roughly similar to the dimensions of agglomerated combustion products of the same material (Fig. 10B). The porosity of the original agglomerates is reduced and pores are seen to be filled by molten Cu-rich material. CuO melts at about 1600 K, a temperature that is expected to be above the ignition point of nano-aluminum. A partially reduced oxide, Cu_2O melts at a lower temperature (ca. 1500 K); it may start forming even before aluminum melts. Even more importantly, the eutectic in the mixed $\text{Al}_2\text{O}_3 - \text{CuO}$ system occurs at around 1100 K (Standards et al. 1981), so that the produced liquid spinel phase (Al_2CuO_4) may block the surface of aluminum, reducing the rate of its further reaction at a much lower temperature. The melt apparently wets the aluminum surface, stabilizing the agglomerates for this material.

Presence of relatively large agglomerates may also explain an inconsistent ignition and large spread among measured pressure values observed for USM powder in Ar, as opposed to air and He. In air, the thermite reaction is assisted by aluminum oxidation with ambient oxygen. Thus,

reaction rate may be high even for porous agglomerated particles, in which aluminum remains exposed to ambient oxygen. In He, the rates of heat and mass transfer are very high, making it easy to ignite particles ejected in a cloud containing burning agglomerates. Conversely, in Ar, the rates of transport processes are low, so that substantial ignition delays may occur for particles ejected from the sample holder. For larger agglomerates, ignition may or may not be achieved, depending on their size and specific direction in which they are ejected. As a result, substantial variation in the measured pressure may be observed.

For the ARM-prepared powder (Fig. 10C), the size of the particles found in combustion products is roughly similar to the sizes of the initial fully dense particles (Fig. 1C). Low-magnification SEM overviews of the collected ARM powders (not shown for brevity) indicated that particles were burning in close proximity of one another; some agglomeration of the burning particles was also observed. The characteristic dimensions of Cu-rich and Al_2O_3 inclusions or clusters were greater than those of the CuO and Al domains in the initial nanocomposite material. This suggests that, as explained earlier, the particles lose their nano-structure upon ignition. The pressure amplitudes for ARM powder are higher in Ar and He (Fig. 9), unlike for ES and USM powders. This may be explained by relative independence of combustion of ARM particles on the presence of the external gas oxidizer. In fact, when ambient oxygen is available, it is likely that in presence of Al or Al_2O_3 , partially reduced CuO forming Cu_2O reoxidizes generating Al_2CuO_4 spinel, which slows down ensuing oxidation of aluminum. This is a kinetic effect, caused by the formation of stable protective layers of the oxidized phases separating Al and CuO. This reoxidation of copper is qualitatively supported by the color of the smoke created by the combustion event. A yellow/green smoke was observed in air, suggesting a mix of various copper oxidation products. However, in both inert environments the smoke was a brilliant red

indicative of a pure metallic copper. In these environments, the lack of external oxidizer may be hypothesized to prevent formation of the spinel, making reaction of Al with CuO and Cu₂O more favorable.

Finally, for the ES powder, the sizes of product particles are noticeably finer than for both USM and ARM materials (Fig. 10A). Individual product particles were relatively far from one another, suggesting no or insignificant agglomeration between them. This is consistent with the ES particle structure, including a gasifying binder (nitrocellulose), which disperses initially agglomerated particles. It is further consistent with the relatively low total mass of the particle loads for this powder. The effect of gas environment on the burn time (time t_{100} for pressure, for example) is the weakest for this powder, suggesting that the gasifying nitrocellulose may actively affect the heat and mass transfer between dispersed Al and CuO particles.

The need for a higher ESD voltage required to ignite the ES powder in He may be explained by combination of small particle sizes, high rate of heat losses due to higher thermal diffusivity if helium, and low initial density of the powder in the sample holder. The particles ignited directly by ESD at 10 kV did not generate sufficient pressure to eject and ignite additional materials.

When the ESD energy was increased (20kV at 10000 pF), more material was ignited directly by ESD, so that the energy produced by the initially ignited cloud was sufficient to lift and ignite more material.

Conclusions

Three powders with the same nominal composition 2Al-3CuO (numbers representing moles) but prepared by different methods, including ultrasonic mixing (USM), electro-spraying (ES), and arrested reactive milling (ARM), were prepared and ignited by ESD. For each powder, experiments were performed in air, argon, and helium. Both USM and ES powders comprised of

porous micron-sized agglomerates of Al and CuO nanoparticles; ARM-prepared particles consisted of micron-sized fully-dense particles in which Al and CuO were mixed on the scale of ~ 100 nm. Combustion temperatures measured for all materials optically were close to their estimated adiabatic flame temperatures and comparable to earlier reported similar materials burning in different configurations. For all materials, combustion times, ranging from 2 to 15 ms were longer than expected for individual nanoparticles but in the range, anticipated for composite particles prepared by ARM or large agglomerates present in the USM powder. The shortest burn times were observed in He consistently for all powders. The ignition delays were longer for the ES powders in all environments, suggesting that the presence of binder delayed thermite reaction initially.

Pressure generated by combustion of powders prepared by ARM increased in the inert environments as compared to that in air; an opposite trend was observed for both USM and ES-prepared powders. This is interpreted considering that the reaction with ambient oxidizer is less important for the fully-dense ARM-prepared particles compared to porous ES and USM materials, in which aluminum is always exposed to the ambient gas. While for ES- and USM materials, ambient oxidizer accelerates oxidation of aluminum, for the ARM powder, in which CuO and Al are mixed in fully-dense composite structures, it causes formation of spinel, Al_2CuO_4 . When produced, spinel is expected to impede further redox reaction, and thus slow down combustion of ARM-prepared powder.

Powders prepared by USM formed large agglomerates; such agglomerates did not react completely and included multiple nano-Al particles bonded by Cu-rich oxidized phase. It appears that partially oxidized melt filled pores, blocking unreacted aluminum from further oxidation. Combustion products of the ARM-prepared powders had dimensions similar to those of the

original material particles. The scale of mixing between Al₂O₃ and Cu-rich phase in the ARM powder combustion products was coarser than that between Al and CuO in the initial material. Combustion products of the ES powders consisted of the finest composite particles; their sizes appeared to be smaller than the sizes of the initial agglomerates observed in the ES powder. Unlike USM powders, the ES-prepared powders burned completely, with the reaction apparently supported by gasifying nitrocellulose binder, which could enhance heat and mass transfer between individual Al and CuO particles in inert environments.

Funding

This work was supported by the US Army Research Office (ARO).

References

- Bockmon, B. S., M. L. Pantoya, S. F. Son, B. W. Asay, and J. T. Mang. 2005. "Combustion velocities and propagation mechanisms of metastable interstitial composites." *Journal of Applied Physics* 98 (6):1-7. doi: 10.1063/1.2058175.
- Comet, M., V. Pichot, B. Siegert, F. Schnell, F. Cizek, and D. Spitzer. 2010. "Phosphorus-based nanothermites: A new generation of energetic materials." *Journal of Physics and Chemistry of Solids* 71 (2):64-68. doi: 10.1016/j.jpcs.2009.07.031.
- Comet, M., B. Siegert, F. Schnell, V. Pichot, F. Cizek, and D. Spitzer. 2010. "Phosphorus-based nanothermites: A new generation of pyrotechnics illustrated by the example of n-CuO/Red P mixtures." *Propellants, Explosives, Pyrotechnics* 35 (3):220-225. doi: 10.1002/prop.201000020.
- Dreizin, E. L. 1996. "Experimental study of stages in aluminum particle combustion in air." *Combustion and Flame* 105 (4):541-556. doi: 10.1016/0010-2180(95)00224-3.

- Dreizin, E. L. 2009. "Metal-based reactive nanomaterials." *Progress in Energy and Combustion Science* 35 (2):141-167. doi: 10.1016/j.peccs.2008.09.001.
- Dreizin, E. L., D. J. Allen, and N. G. Glumac. 2014. "Depression of melting point for protective aluminum oxide films." *Chemical Physics Letters* 618:63-65.
- Dreizin, E. L., C. Badiola, S. Zhang, and Y. Aly. 2011. "Particle Combustion Dynamics of Metal-Based Reactive Materials." *International Journal of Energetic Materials and Chemical Propulsion* 10 (4):22.
- Dreizin, E.L., and M. Schoenitz. 2009. Nano-composite energetic powders prepared by arrested reactive milling. In *US Patent 7,524,355*
- Dreizin, Edward L., and Mirko Schoenitz. 2014. "Reactive and Metastable Nanomaterials Prepared by Mechanical Milling." In *Metal Nanopowders*, 227-278. Wiley-VCH Verlag GmbH & Co. KGaA.
- Dutro, G. M., R. A. Yetter, G. A. Risha, and S. F. Son. 2009. "The effect of stoichiometry on the combustion behavior of a nanoscale Al/MO₃ thermite." *Proceedings of the Combustion Institute* 32 II:1921-1928. doi: 10.1016/j.proci.2008.07.028.
- Goroshin, S., J. Mamen, A. Higgins, T. Bazyn, N. Glumac, and H. Krier. 2007. "Emission spectroscopy of flame fronts in aluminum suspensions." Heidelberg.
- Jacob, Rohit J., Guoqiang Jian, Philip M. Guerieri, and Michael R. Zachariah. 2015. "Energy release pathways in nanothermites follow through the condensed state." *Combustion and Flame* 162 (1):258-264. doi: 10.1016/j.combustflame.2014.07.002.
- Jacob, Rohit J., Boran Wei, and Michael R. Zachariah. 2015. "Quantifying the enhanced combustion characteristics of electrospray assembled aluminum mesoparticles." *Combustion and Flame*. doi: 10.1016/j.combustflame.2015.09.032.

- Kim, S. H., and M. R. Zachariah. 2004. "Enhancing the rate of energy release from nanoenergetic materials by electrostatically enhanced assembly." *Advanced Materials* 16 (20):1821-1825. doi: 10.1002/adma.200306436.
- Li, X., P. Guerieri, W. Zhou, C. Huang, and M. R. Zachariah. 2015. "Direct deposit laminate nanocomposites with enhanced propellant properties." *ACS Applied Materials and Interfaces* 7 (17):9103-9109. doi: 10.1021/acsami.5b00891.
- McBride, B.J., and S. Gordon. 1996. Computer Program for Calculation of Complex Chemical Equilibrium Compositions and Applications II. Users Manual and Program Description. NASA RP 1311.
- Monk, I., M. Schoenitz, and E.L. Dreizin. 2016. "Modes of ignition of powder layers of nanocomposite thermites by electro-static discharge." *Journal of Energetic Materials* in Press. doi: 10.1080/07370652.2016.1150366.
- Monk, I., R. Williams, X. Liu, and E. L. Dreizin. 2015. "Electro-static discharge ignition of monolayers of nanocomposite thermite powders prepared by arrested reactive milling." *Combustion Science and Technology* 187 (8):1276-1294. doi: 10.1080/00102202.2015.1035373.
- Pantoya, M. L., and J. J. Granier. 2005. "Combustion behavior of highly energetic thermites: Nano versus micron composites." *Propellants, Explosives, Pyrotechnics* 30 (1):53-62. doi: 10.1002/prop.200400085.
- Reese, D. A., D. M. Wright, and S. F. Son. 2013. "CuO/Al thermites for solid rocket motor ignition." *Journal of Propulsion and Power* 29 (5):1194-1199. doi: 10.2514/1.B34771.
- Sanders, V. E., B. W. Asay, T. J. Foley, B. C. Tappan, A. N. Pacheco, and S. F. Son. 2007. "Reaction propagation of four nanoscale energetic composites (Al/MO₃, Al/WO₃,

- Al/CuO, and Bi₂O₃)." *Journal of Propulsion and Power* 23 (4):707-714. doi: 10.2514/1.26089.
- Schoenitz, M., T. S. Ward, and E. L. Dreizin. 2005. "Arrested reactive milling for in-situ production of energetic nanocomposites for propulsion and energy-intensive technologies in exploration missions." Reno, NV.
- Son, S. F., B. W. Asay, T. J. Foley, R. A. Yetter, M. H. Wu, and G. A. Risha. 2007. "Combustion of nanoscale Al/MoO₃ thermite in microchannels." *Journal of Propulsion and Power* 23 (4):715-721. doi: 10.2514/1.26090.
- Spitzer, D., M. Comet, C. Baras, V. Pichot, and N. Piazzon. 2010. "Energetic nano-materials: Opportunities for enhanced performances." *Journal of Physics and Chemistry of Solids* 71 (2):100-108.
- Standards, United States. National Bureau of, American Ceramic Society, Institute for Materials Science, Engineering . Ceramics Division, Materials Science, and Engineering Laboratory . Ceramics Division. 1981. *Phase Diagrams for Ceramists*: American Ceramic Society.
- Sun, J., M. L. Pantoya, and S. L. Simon. 2006. "Dependence of size and size distribution on reactivity of aluminum nanoparticles in reactions with oxygen and MoO₃." *Thermochimica Acta* 444 (2):117-127. doi: 10.1016/j.tca.2006.03.001.
- Wang, H., J. B. DeLisio, G. Jian, W. Zhou, and M. R. Zachariah. 2015. "Electrospray formation and combustion characteristics of iodine-containing Al/CuO nanothermite microparticles." *Combustion and Flame* 162 (7):2823-2829. doi: 10.1016/j.combustflame.2015.04.005.

- Wang, H., G. Jian, G. C. Egan, and M. R. Zachariah. 2014. "Assembly and reactive properties of Al/CuO based nanothermite microparticles." *Combustion and Flame* 161 (8):2203-2208. doi: 10.1016/j.combustflame.2014.02.003.
- Weismiller, M. R., J. G. Lee, and R. A. Yetter. 2011. "Temperature measurements of Al containing nano-thermite reactions using multi-wavelength pyrometry." *Proc. Combust. Inst.* 33 (Copyright (C) 2015 American Chemical Society (ACS). All Rights Reserved.):1933-1940. doi: 10.1016/j.proci.2010.06.094.
- Williams, R. A., E. Beloni, and E. L. Dreizin. 2012. "Ignition of metal powder layers of different thickness by electrostatic discharge." *Journal of Propulsion and Power* 28 (1):132-139. doi: 10.2514/1.b34231.
- Williams, R. A., J. V. Patel, and E. L. Dreizin. 2014. "Ignition of fully dense nanocomposite thermite powders by an electric spark." *Journal of Propulsion and Power* 30 (3):765-774. doi: 10.1016/0304-3886(85)90041-5.
- Yetter, R. A., G. A. Risha, and S. F. Son. 2009. "Metal particle combustion and nanotechnology." *Proceedings of the Combustion Institute* 32 II:1819-1838. doi: 10.1016/j.proci.2008.08.013.
- Young, G., H. Wang, and M. R. Zachariah. 2015. "Application of nano-aluminum/nitrocellulose mesoparticles in composite solid rocket propellants." *Propellants, Explosives, Pyrotechnics* 40 (3):413-418. doi: 10.1002/prop.201500020.

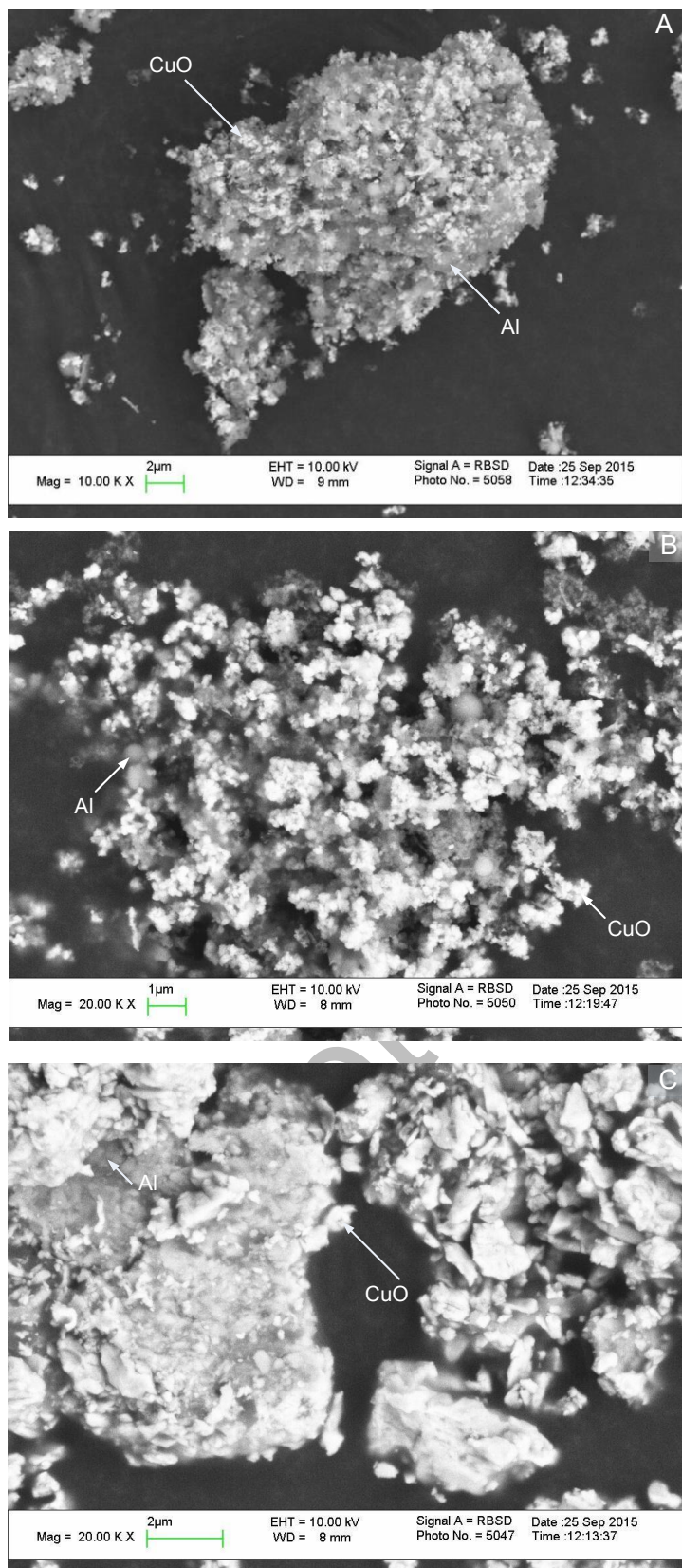


Figure 1. SEM images of different 2Al-3CuO nanocomposite powders: A: ES, B: USM; C: ARM.

Table 1. The percent of powder ejected upon ESD ignition.

| Composite type | Loading Density (g/cm ³) | Percent of 2Al-3CuO lost after ignition | | |
|----------------|--------------------------------------|---|------------|------------|
| | | Environment | | |
| | | Air | Argon | Helium |
| ES | 0.080 ± 0.012 | 76.1 ± 9.0 | 83.6 ± 8.9 | 90.3 ± 6.0 |
| USM | 0.13 ± 0.04 | 91.8 ± 2.9 | 85.7 ± 7.8 | 87.5 ± 2.1 |
| ARM | 0.32 ± 0.03 | 88.2 ± 1.2 | 87.6 ± 1.1 | 82.9 ± 2.9 |

Accepted Manuscript

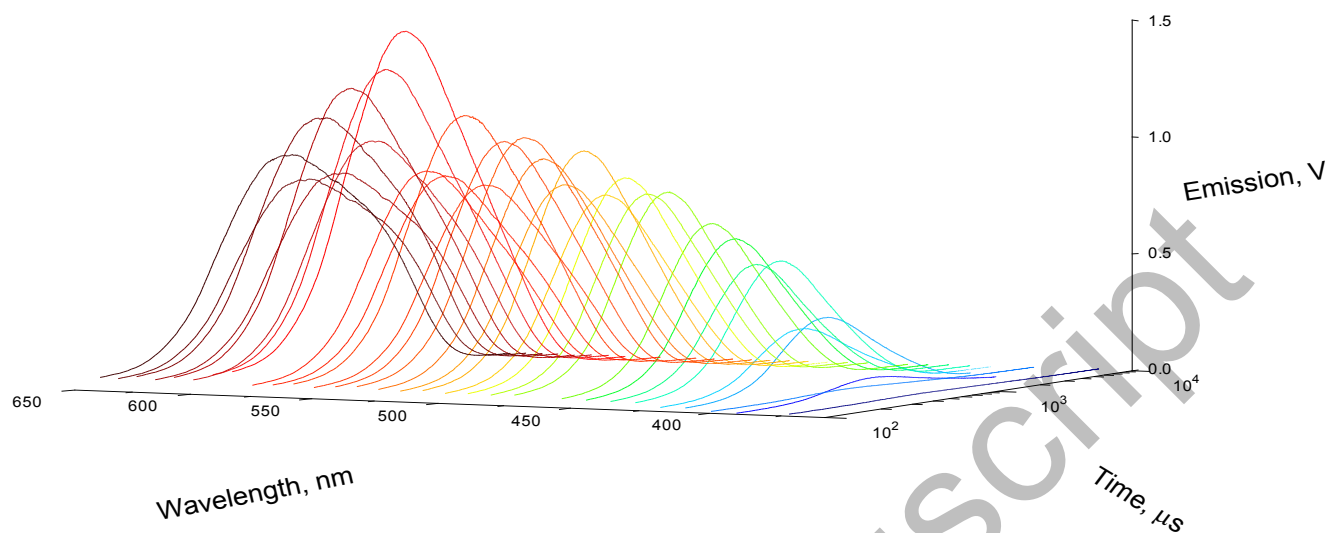


Figure 2. Characteristic emission traces recorded using the 32-channel spectrometer for a USM-prepared 2Al-3CuO nanocomposite thermite ignited in air.

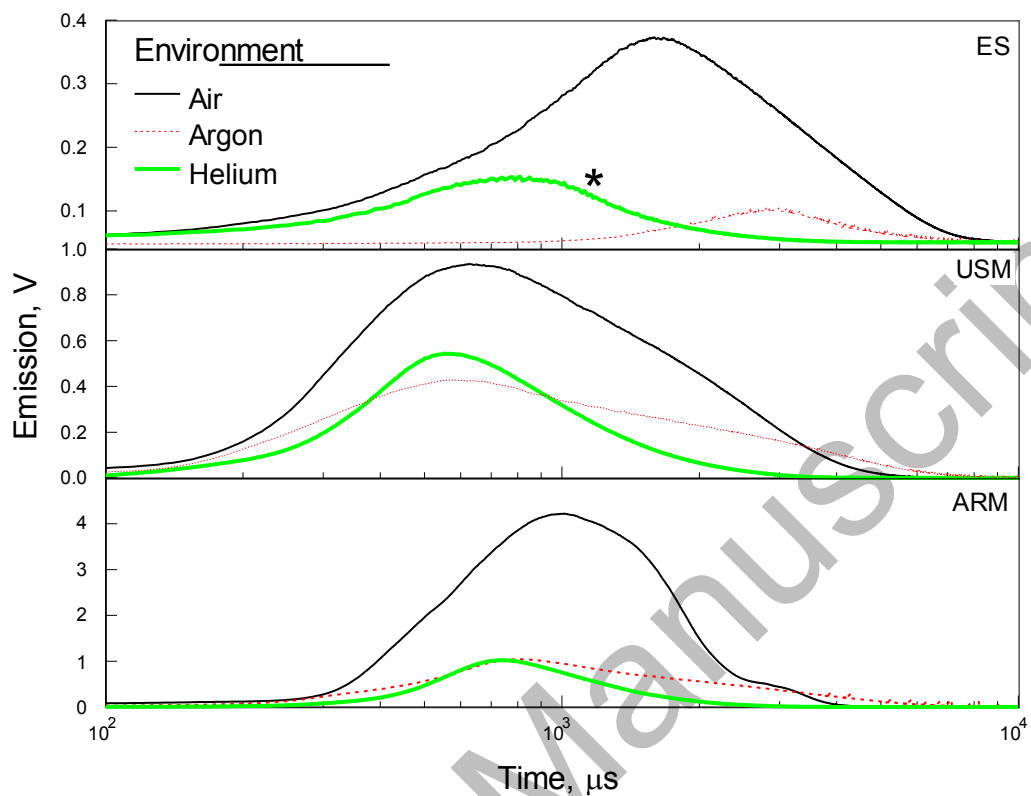


Figure 3. Emission traces (567.7nm) for different nanocomposite thermite powders ignited by ESD in different environments.

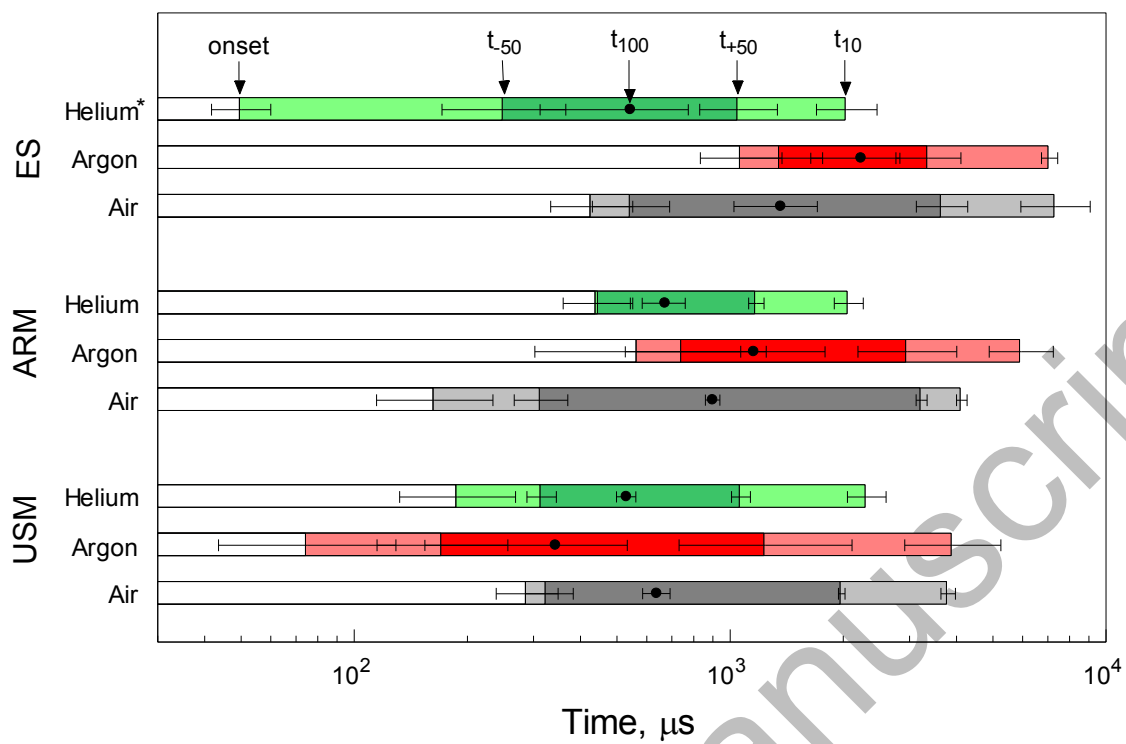


Figure 4. Temporal characteristics of emission pulses produced by ESD-ignited Al-CuO powders at 567.7 nm wavelength in various environments.

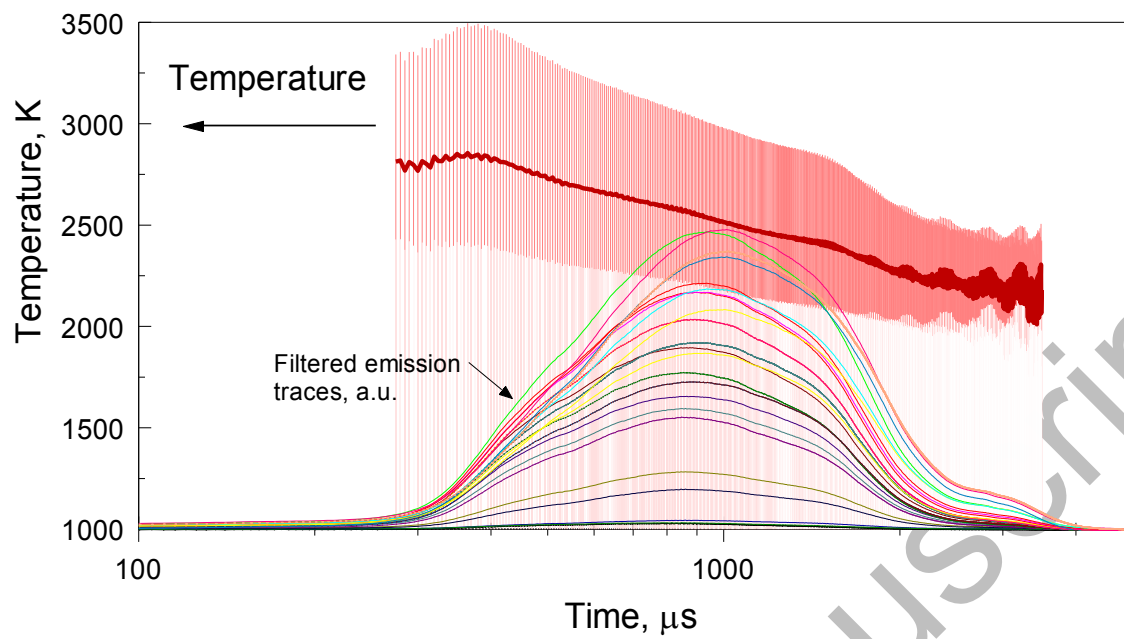


Figure 5. Temperature (in bold red) overlaid with filtered emission traces for ARM-powder.

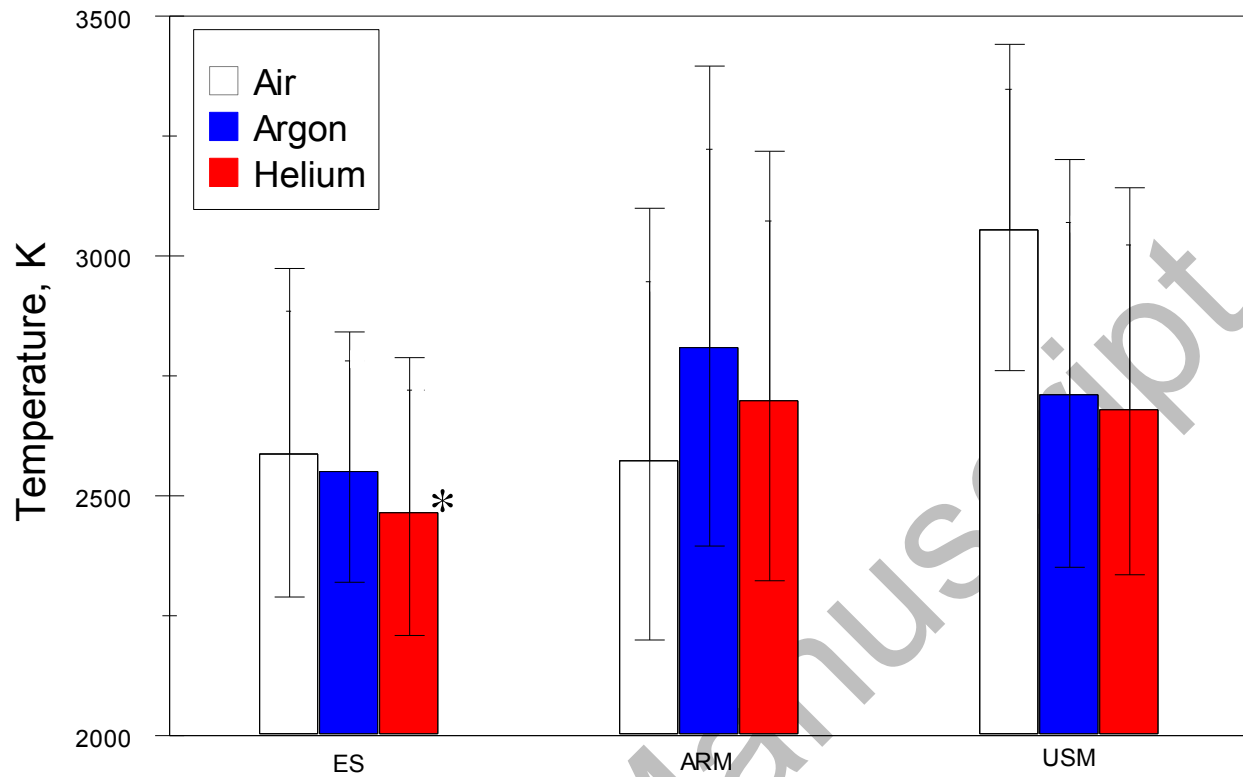


Figure 6. Temperatures taken at the emission peak measured for the 567.7-nm emission for different materials ignited in different environments.

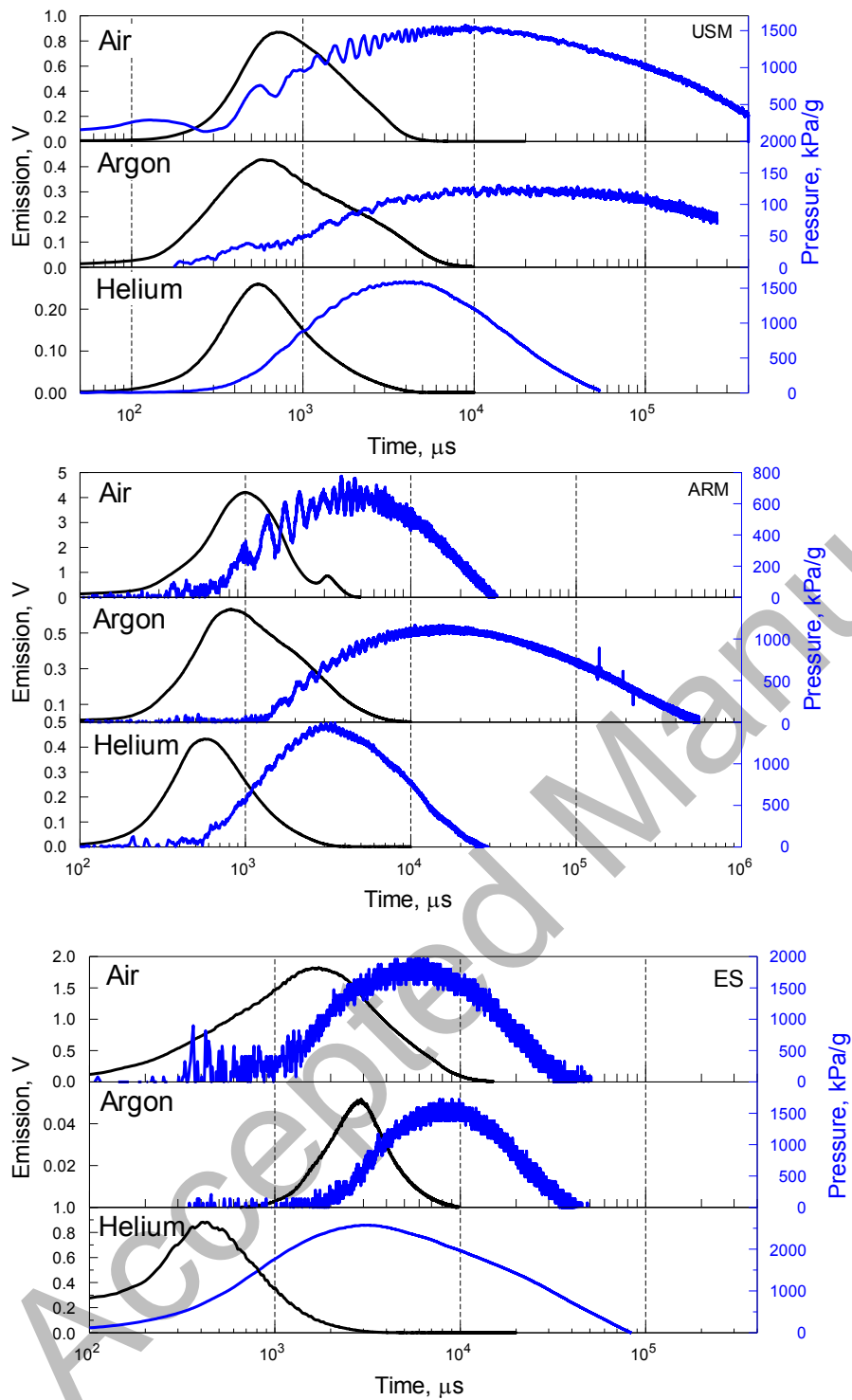


Figure 7. Pressure traces (thick blue lines) overlaid with emission traces for all environments and materials.

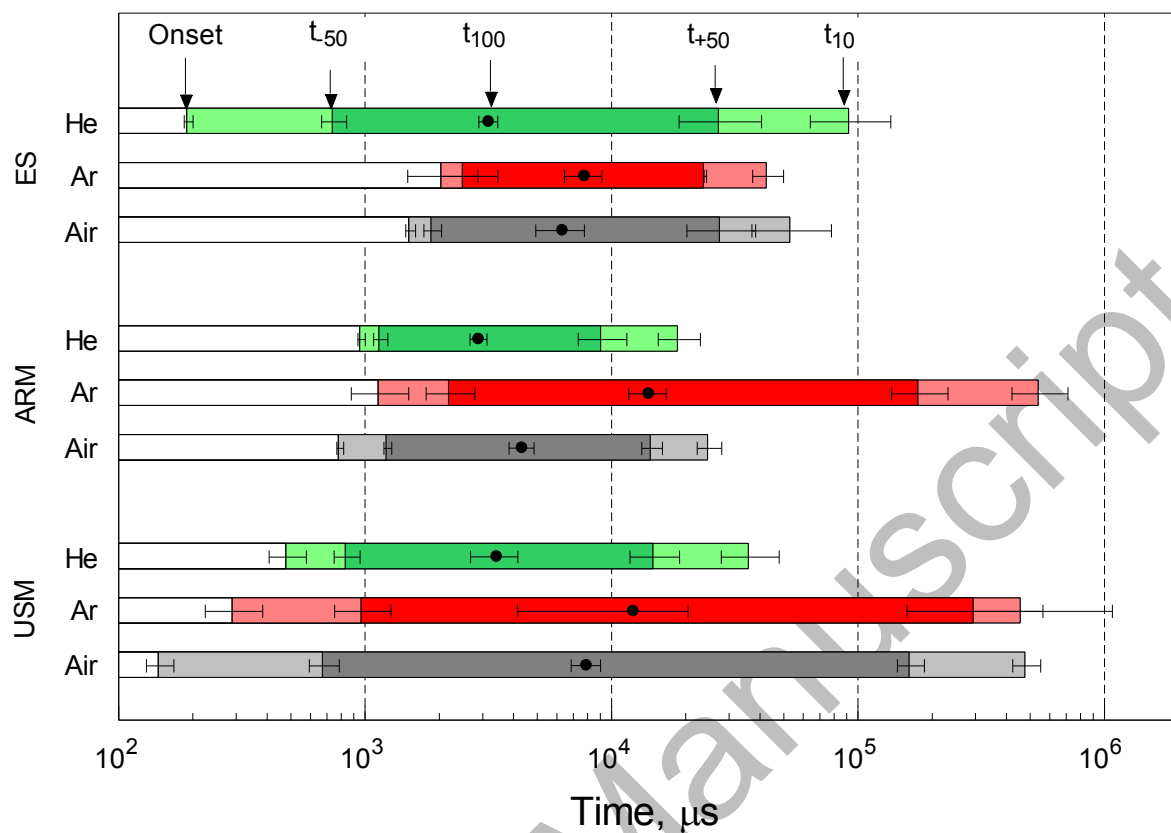


Figure 8. Temporal characteristics for pressure traces for all powders in different environments.

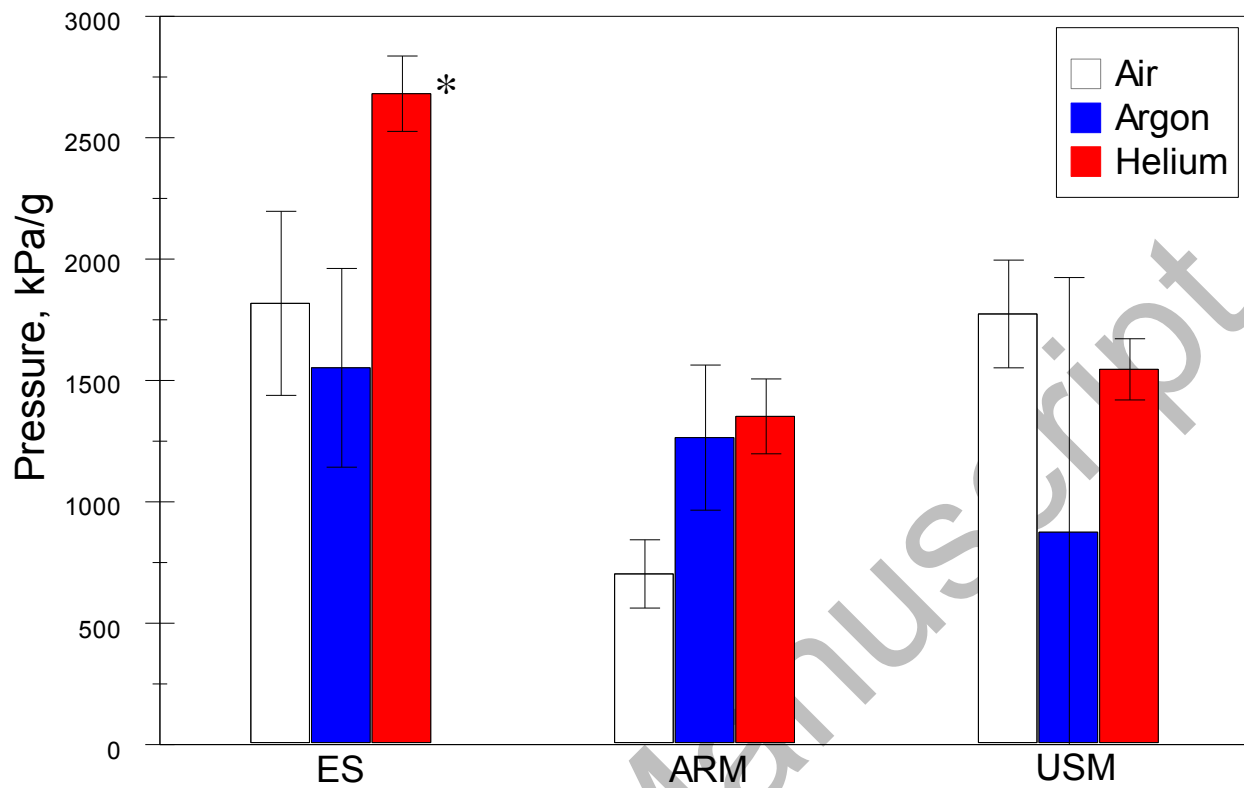


Figure 9. Maximum normalized pressures obtained from the ESD ignition of various Al-CuO powders in different environments.

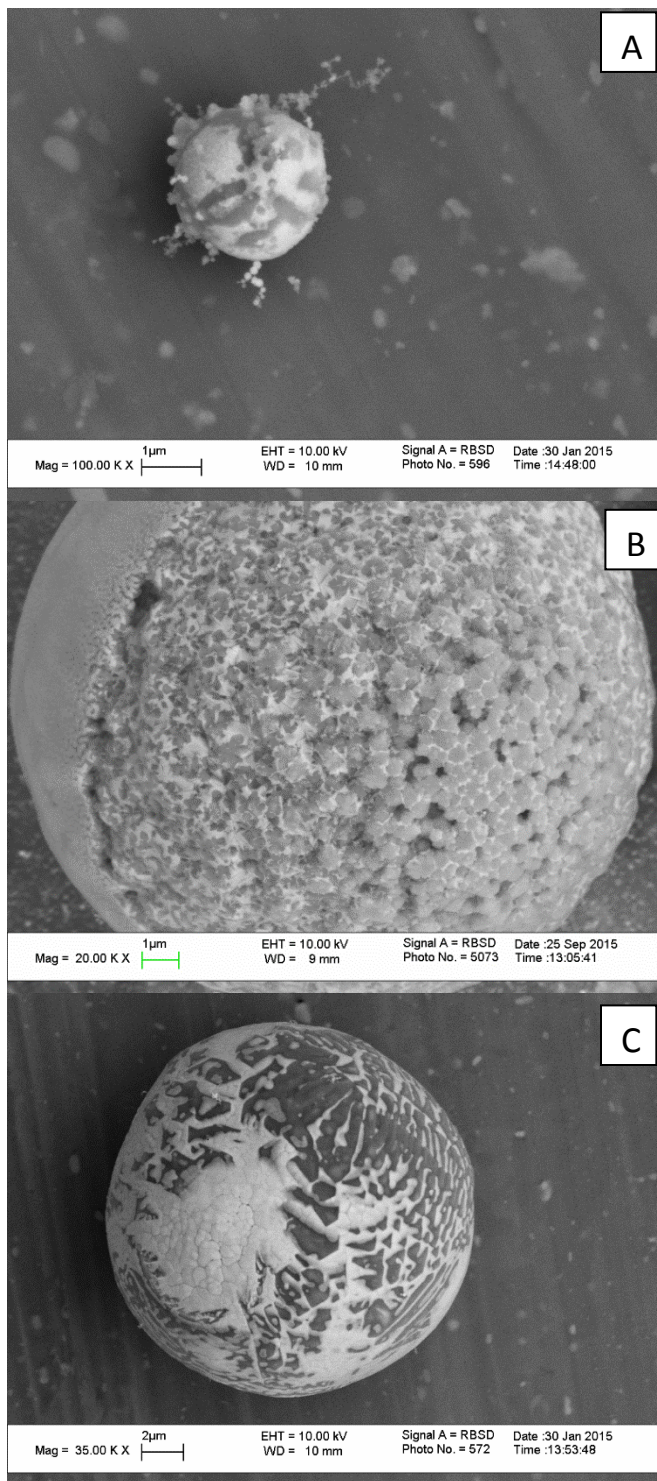


Figure 10. SEM images of combustion products of different 2Al-3CuO powders ignited in air. A: ES; B: USM; C: ARM.